

# Evaluating Disentanglement of Structured Latent Representations

Raphaël Dang-Nhu<sup>1</sup> Angelika Steger<sup>2</sup>

## Abstract

We design the first multi-layer disentanglement metric operating at all hierarchy levels of a structured latent representation, and derive its theoretical properties. Applied to object-centric representations, our metric unifies the evaluation of both object separation between latent slots and internal slot disentanglement into a common mathematical framework. It also addresses the problematic dependence on segmentation mask sharpness of previous pixel-level segmentation metrics such as ARI. Perhaps surprisingly, our experimental results show that good ARI values do not guarantee a disentangled representation, and that the exclusive focus on this metric has led to counterproductive choices in some previous evaluations. As an additional technical contribution, we present a new algorithm for obtaining feature importances that handles slot permutation invariance in the representation.

## 1. Introduction

A salient challenge in the field of feature learning is the ability to decompose the representation of images and scenes into distinct objects that are generated separately and then combined together. Indeed, the capacity to reason about objects and their relations is a central aspect of human intelligence (Spelke et al., 1992) that can be used in conjunction with graph neural networks to enable efficient relational reasoning and improve existing AI systems (Lake et al., 2017; Wang et al., 2018; Watters et al., 2019; Battaglia et al., 2018; Brunton et al., 2020). In the last years, several models have been proposed that learn a compositional representation for images: TAGGER (Greff et al., 2016), NEM (Greff et al., 2017), R-NEM (Van Steenkiste et al., 2018), MONet (Burgess et al., 2019), IODINE (Greff et al., 2019), GENESIS (Engelcke et al., 2019), Slot Attention (Locatello et al., 2020), MulMON (Li et al., 2020), SPACE (Lin et al., 2020). These models have to jointly learn how to

<sup>1</sup>INRIA <sup>2</sup>ETH Zürich. Correspondence to: Raphaël Dang-Nhu <raphael.dangnhu@gmail.com>.

represent individual objects and how to segment the image into different components, the latter sometimes being referred to as perceptual grouping. They all share a number of common principles: (i) Split the latent representation into several groups of dimensions, also known as *slots*. (ii) Inside each slot, encode information about both pixel group assignments and individual object representation. (iii) Maintain a symmetry between slots in order to respect the permutation invariance of objects composition.

In order to compare algorithms and select models, it is indispensable to have robust disentanglement metrics. At the level of individual factors of variations, a representation is said to be disentangled when information about the different factors is separated between different latent dimensions (Bengio et al., 2013; Locatello et al., 2019). At object-level, disentanglement measures the degree of object separation between slots. However, all existing metrics (Higgins et al., 2016; Kim & Mnih, 2018; Chen et al., 2018; Ridgeway & Mozer, 2018; Eastwood & Williams, 2018; Kumar et al., 2017) are limited to the individual case, which disregards the representation structure. To cite Kim & Mnih (2018) about the FactorVAE metric:

The definition of disentanglement we use [...] is clearly a simplistic one. It does not allow correlations among the factors or hierarchies over them. Thus this definition seems more suited to synthetic data with independent factors of variation than to most realistic datasets.

As a result, prior work has restricted to measuring the degree of object separation via pixel-level segmentation metrics. Most considered is the Adjusted Rand Index (Rand, 1971; Greff et al., 2019), a measure of clustering similarity than can be applied to object separation by considering pixel segmentation as a cluster assignment. Other metrics such as Segmentation Covering (Arbelaez et al., 2010) have been introduced to penalize over-segmentation of objects. A fundamental limitation is that they do not evaluate directly the quality of the representation, but instead consider a visual proxy of object separation. This results in problematic dependence on the quality of the inferred segmentation masks. For instance, the authors of IODINE (Greff et al., 2019) noticed that the low ARI of their model on the Multi-dSprites

dataset is mostly due to unsharp segmentation masks, despite good object separation. Moreover, our experimental results show that is possible to obtain near perfect ARI without actually learning a satisfying representation.

To address these limitations, we present the first structured disentanglement metric operating at different levels of hierarchy in the data generating process. Applied to object-centric representations, our method mathematically unifies the evaluation of object separation between slots and of internal slot disentanglement. It naturally extends to data generating processes and representations with arbitrary hierarchies. Moreover, it is mathematically elegant and prone to theoretical analysis: We leverage information theoretic inequalities to understand the behavior of our metric when combining hierarchy levels. Our key theoretical result is that our multi-level framework provide a sound substitute for prior disentanglement metrics. Experimentally, we compare the representations learned by three architectures: MONet, GENESIS and IODINE. The results confirm issues with pixel-level segmentation metrics and show that our metric offers a potential solution. They also offer additional insight about the respective strengths of the different models.

## 2. Background and Definitions

### 2.1. Disentanglement criteria

There exists an extensive literature discussing notions of disentanglement, accounting for all the different definitions is outside the scope of this paper. We chose to focus on the three criteria formalized by [Eastwood & Williams \(2018\)](#), which stand out because of their clarity and simplicity. *Disentanglement* is the degree to which a representation separates the underlying factors of variation, with each latent variable capturing at most one generative factor. *Completeness* is the degree to which each underlying factor is captured by a single code variable. *Informativeness* is the amount of information that a representation captures about the underlying factors of variation. Similarly to prior work, the word *disentanglement* is also used as a generic term that simultaneously refers to these three criteria. In the following, it should be clear depending on the context whether it is meant as general or specific.

### 2.2. The DCI metric

For brevity reasons, we only describe the DCI metric ([Eastwood & Williams, 2018](#)), which is most closely related to our work. The supplementary material provides a comprehensive overview of existing disentanglement metrics.

Consider a dataset  $\mathcal{X}$  composed of  $N$  observations  $x^1, \dots, x^N$ , which we assume are generated by combining  $F$  underlying factors of variation. The value of the different

factors for observation  $x^l$  are denoted  $v_1^l, \dots, v_F^l$ . Suppose we have learned a representation  $z = (z_1, \dots, z_L)$  from this dataset. The DCI metric is based on the affinity matrix  $R = (R_{i,j})$ , where  $R_{i,j}$  measures the relative importance of latent  $z_i$  in predicting the value of factor  $v_j$ . Supposing an appropriate normalization for the matrix, disentanglement is measured as the weighted average of the matrix' row entropy. Conversely, completeness is measured as the weighted average of column entropy. Finally, informativeness is measured as the normalized error of the predictor used to obtain the matrix  $R$ .

### 2.3. Our relational setting

The specificity of our setting compared to the DCI metric is that the structured organization of latent variables and factors of variations can not be accurately described by scalar indexes. We propose a formalization of such structures in the most general way via *relational indexing*, illustrated on a toy example in the next subsection. This consists in replacing the scalar ranging from 1 to  $F$  with a set of tuples  $\tau \in \mathcal{T}$ . The factors' values for sample  $i$  can thus be denoted  $(v_\tau^i)_{\tau \in \mathcal{T}}$ . Similarly for the representation  $z$ , we replace the scalar ranging from 1 to  $K$  with a set of tuples  $\hat{\tau} \in \hat{\mathcal{T}}$ . The dimensions of  $z$  can be written  $z = (z_{\hat{\tau}})_{\hat{\tau} \in \hat{\mathcal{T}}}$ . We denote  $|\mathcal{T}| = F$  and  $|\hat{\mathcal{T}}| = L$ . Intuitively, the structure on factors given by  $\mathcal{T}$  expresses the goal of metric (e.g. measuring object separation). The structure on latent dimensions given by  $\hat{\mathcal{T}}$  depends on the model architecture. In the case of object-centric representations,  $\hat{\mathcal{T}}$  accounts for the fact that the representations is obtained by concatenating different groups of latent dimensions, known as slots.

Formally, both relations are defined with respect to  $n$  level attributes  $A_1, \dots, A_n$ . Each attribute is associated with a set of possible values (a domain) for factors  $\text{dom}_F(A_i)$  and for latents  $\text{dom}_L(A_i)$ . These domains constrain the possible values for the tuple indexes, such that  $\mathcal{T} \subset \prod_{i=1}^n \text{dom}_F(A_i)$ , and  $\hat{\mathcal{T}} \subset \prod_{i=1}^n \text{dom}_L(A_i)$ . Concretely, each attribute is responsible for one level of the hierarchy. As an illustration, in the case of object-centric generative models,  $A_1$  is responsible for the object/slot hierarchy level, while  $A_2$  is responsible for the internal object properties and slot representation.

### 2.4. Toy example

For a toy data generating process with two objects having two properties each, examples relations for these attributes are

$$\mathcal{T} = \{( \text{object 1, color}), ( \text{object 1, size}), \\ ( \text{object 2, color}), ( \text{object 2, size})\},$$

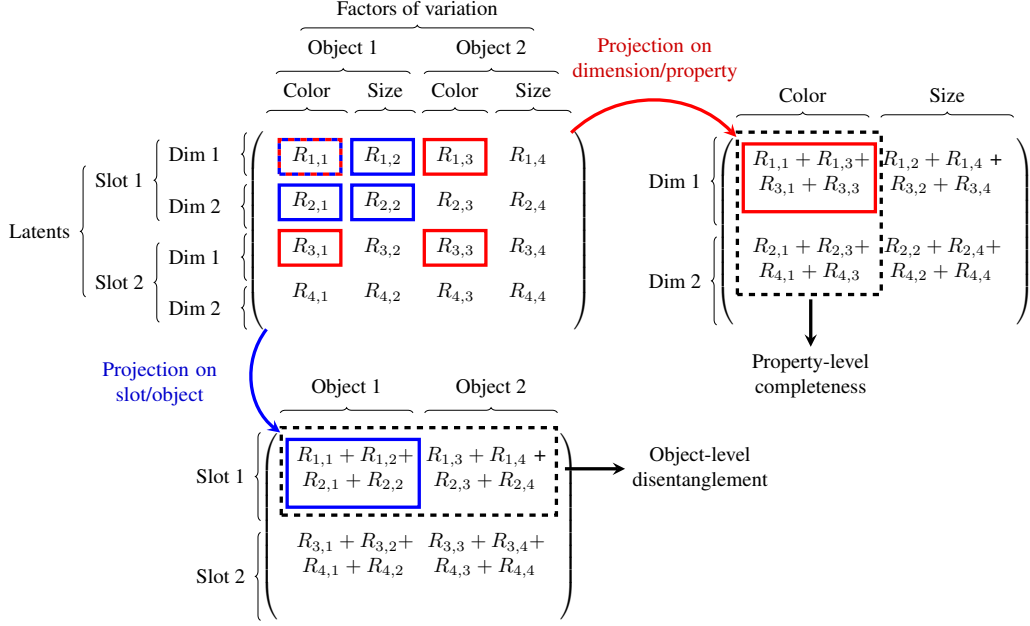


Figure 1. Illustration of the metric on the toy example of Section 2. It operates as a two stage process: (i) A projection step where the affinity scores are grouped and summed according to the projection of factors and latents. (ii) An evaluation step where the row (resp. column) entropy yields a measurement of disentanglement (resp. completeness). We suppose appropriate coefficient normalization.

and

$$\hat{\mathcal{T}} = \{(slot 1, dim 1), (slot 1, dim 2), (slot 2, dim 1), (slot 2, dim 2)\}$$

### 3. Measuring Multi-Level Disentanglement

#### 3.1. High-level presentation

Prior metrics have focused on measuring disentanglement at the level of individual factors of variation and latent dimensions. On top of this traditional disentanglement property (that we will refer as *global* or *unstructured* disentanglement), additional characteristics are desirable in the case of representations with multiple objects slots:

**Object-level disentanglement:** The information about one object should be contained in single slot, i.e. changing one object should lead to changes in a single slot, and vice-versa. This corresponds to disentanglement at object level.

**Slot symmetry:** The latent dimension responsible for a given factor (e.g., color) should be invariant across slots. This means that slots should have the same inner structure, implying a form of permutation invariance across objects.

**Slot disentanglement:** The internal slot representation must disentangle the factors related to a given object.

Our multi-level disentanglement metric allows to evaluate these criteria within a unified framework. In line with prior

work, it is based on the affinity score  $R_{\hat{\tau}, \tau}$  measuring the relative importance of  $z_{\hat{\tau}}$  in predicting  $v_{\tau}$ . The key novelty is that we propose to measure disentanglement with respect to an arbitrary **projection** (Codd, 2002) of the relational indexes and affinity matrix. Projecting a relation corresponds to selecting a subset of the attributes while discarding the rest, and update the relation's tuples by removing the values corresponding to the deleted attributes. This results in potential duplicate tuples being merged together.

Intuitively, projections are a way to consider a subset of the organization levels in the factors of variations and latent space. In the case of object-centric representations, projecting along the first object attribute allows to study the relations of objects and slots without taking their internal structure into consideration. Ultimately this permits to evaluate our object-level disentanglement criterion. Inversely, projecting along the second attribute allows to study the internal slot representation independently of the object, leading to evaluation of both internal slot disentanglement and slot symmetry. Finally, global disentanglement is examined by means of the trivial projection conserving all attributes.

An important question concerning our metric is to determine how to adapt affinity scores when projecting, as these are originally only defined for pairs of factors of variation and latent dimension. We chose to sum the scores for duplicate entries. This allows for preservation of the

normalization, and ensures a form of compositionality and commutativity with respect to successive projections. Moreover, this permits a natural and concise extension of the entropy measure of disentanglement. The two-step process of projection and measure of disentanglement on the projected affinity matrix is illustrated in Figure 1.

Finally, we had to solve some specific issues in order to get suitable affinity scores for object-centric latent representations. We developed an algorithm for obtaining feature importance that are permutation invariant with respect to slots. Indeed, the architectures we considered do not yield a deterministic ordering for their object decomposition. This contribution is presented separately in Section 4.

### 3.2. Definition of the metric

The mathematical formalization of our metric builds on a probabilistic view of the affinity matrix as a joint random variable  $(X, Y)$ , where  $X$  is a random latent dimension, and  $Y$  a random factor. Supposing that the affinity coefficients  $(R_{\hat{\tau}, \tau})$  are normalized to sum up to one, we can define a joint random variable  $(X, Y)$  having values in  $\hat{\mathcal{T}} \times \mathcal{T}$  with probability

$$\mathbb{P}[X = \hat{\tau}, Y = \tau] = R_{\hat{\tau}, \tau}.$$

As a consequence, the conditional probability  $\mathbb{P}[X = \hat{\tau} | Y = \tau]$  can be computed as follows

$$\mathbb{P}[X = \hat{\tau} | Y = \tau] = \frac{R_{\hat{\tau}, \tau}}{\sum_{i \in \hat{\mathcal{T}}} R_{i, \tau}}.$$

The conditional probability  $\mathbb{P}[Y = \tau | X = \hat{\tau}]$  has a symmetric form. We will see in Theorem 1 that this probabilistic view yields a mathematically elegant formulation of the metrics that subsumes the DCI framework. An additional benefit of this formalism is the availability of standard information-theoretic identities and inequalities that make it much more convenient to derive the metric properties. Next, we define the formal meaning of a projection.

**Definition 1** (Projection). *Consider a relation over  $n$  attributes, and a set of indices  $i = \{e_1, \dots, e_l\}$ , where  $1 \leq e_1 < \dots < e_l \leq n$ . The projection  $\rho_i(\tau)$  of a tuple  $\tau = (\tau_1, \dots, \tau_n)$  on this relation is defined as*

$$\rho_i(\tau) = (\tau_{e_1}, \dots, \tau_{e_l}).$$

*The projection of a relation is obtained by projecting all tuples on the relation. That is,*

$$\rho_i(\mathcal{T}) = \{\rho_i(\tau) ; \tau \in \mathcal{T}\}.$$

Now we are ready to define our multi-level metrics. In the following,  $H_U(A|B)$  denotes the conditional entropy of  $A$

with respect to  $B$  in base  $U$ , while  $I_U(A; B|C)$  denotes the mutual information of  $A$  and  $B$  conditioned on  $C$ . Formal definitions and properties of these information-theoretic quantities are given in the supplementary.

**Completeness** Given a projection  $i$ , the completeness with respect to this projection measures how well the projected factors are captured by a coherent group of latent variables, by measuring column entropy in the projected space. It is measured as

$$C(i) = 1 - H_U(\rho_i(X) | \rho_i(Y)),$$

where  $U = |\rho_i(\hat{\mathcal{T}})|$  is the number of groups of latents in the projection.

**Disentanglement** Given a projection  $i$ , the disentanglement with respect to this projection measures to what extent a group of latent variables influences a coherent subset of factors of variation, by measuring line entropy in the projected space. It is measured as

$$D(i) = 1 - H_V(\rho_i(Y) | \rho_i(X)),$$

where  $V = |\rho_i(\mathcal{T})|$  is the number of groups of factors in the projection.

**Informativeness** Our informativeness metric remains global, and thus similar to the DCI framework. However, we found it interesting in some cases to average informativeness over projected groups, in order to provide more interpretable results.

### 3.3. Theoretical results

In this section, we present a theoretical analysis of the properties of our metric when combining hierarchy levels. The main interest of these results is to formally show that the metrics associated with individual hierarchy levels provide a **sound substitute for prior unstructured metrics**. Our main result, Theorem 2, shows that if all individual hierarchy levels are perfectly disentangled, then unstructured DCI disentanglement is also perfect. Applied to object-centric representations, this means that a model obtaining perfect object-level and property-level metrics also achieves perfect global disentanglement values. This makes the unstructured DCI metric redundant with our framework, and allows us to restrict to a small number of interpretable metrics related to individual hierarchy levels.

This result has a reciprocal, but it comes in form of a weaker bound (Theorem 3), which is not totally controllable. Intuitively, this is due to the fact that our metrics convey strictly more information than the unstructured DCI framework. For brevity reasons, we only put the statement of our theoretical results in the main paper. Detailed proofs can be found in

the supplementary material. Our first result formalizes the connection with the DCI metric framework.

**Theorem 1.** *With the total projection  $i = \{1, \dots, n\}$ , our metric captures the disentanglement and completeness metrics of the DCI framework (Eastwood & Williams, 2018).*

In Definition 2, we define a notation for joining projections and hierarchy levels. Theorem 2 provides a strong lower bound for the joint metric, while Theorem 3 provide a matching upper bound.

**Definition 2** (Union of projections). *Consider  $k$  disjunct projections  $i^1 = \{e_1^1, \dots, e_{l_1}^1\}, \dots, i^k = \{e_1^k, \dots, e_{l_k}^k\}$  of the generative model. The union of these projections is defined as*

$$i = \bigcup_{s=1}^k i^s.$$

*It is a projection of size  $l_1 + \dots + l_k$ .*

**Theorem 2** (Lower bound). *Consider  $k$  disjunct projections  $i^1, \dots, i^k$  with respectively  $L^1, \dots, L^k$  groups of latents and  $F^1, \dots, F^k$  groups of factors. Moreover, assume that the joint projection  $i = \bigcup_{s=1}^k i^s$  has  $L$  groups of latents and  $F$  groups of factors. The following lower bound for the joint completeness holds*

$$1 - k + \sum_{s=1}^k C(i^s) \leq 1 - \sum_{s=1}^k \frac{1 - C(i^s)}{\log_{L^s}(L)} \leq C \left( \bigcup_{s=1}^k i^s \right).$$

*Similarly, we have for the disentanglement metric*

$$1 - k + \sum_{s=1}^k D(i^s) \leq 1 - \sum_{s=1}^k \frac{1 - D(i^s)}{\log_{F^s}(F)} \leq D \left( \bigcup_{s=1}^k i^s \right).$$

In particular, the previous theorem allows to lower bound the global disentanglement (resp. completeness) (projection  $i = \{1, \dots, n\}$ ) with the disentanglement (resp. completeness) of single attribute projections  $\{1\}, \dots, \{n\}$ . Suppose that all the individual projections verify  $D(\{s\}) \geq 1 - \epsilon$ , where  $\epsilon \geq 0$ . Then we obtain the lower bound  $D(i) \geq (1 - n) + n(1 - \epsilon) = 1 - n\epsilon$ . In the case of object-centric representations, this means that the object-level disentanglement and internal slot disentanglement provide a lower bound for global unstructured disentanglement.

**Theorem 3** (Upper bound). *Consider  $k$  disjunct projections  $i^1, \dots, i^k$  with respectively  $L^1, \dots, L^k$  groups of latents and  $F^1, \dots, F^k$  groups of factors. Moreover, assume that the joint projection  $i = \bigcup_{s=1}^k i^s$  has  $L$  groups of latents and  $F$  groups of factors. The following upper bound for the completeness metric holds*

$$C \left( \bigcup_{s=1}^k i^s \right) \leq 1 - \max_{1 \leq s \leq k} \left( \frac{1 - C(i^s)}{\log_{L^s}(L)} - A_s \right),$$

where

$$A_s = I_L \left( \rho_{i^s}(X); \rho \bigcup_{t \neq s} i^t(Y) \mid \rho_{i^s}(Y) \right).$$

Similarly, we have for the disentanglement metric that

$$D \left( \bigcup_{s=1}^k i^s \right) \leq 1 - \max_{1 \leq s \leq k} \left( \frac{1 - D(i^s)}{\log_{F^s}(F)} - B_s \right).$$

where

$$B_s = I_F \left( \rho_{i^s}(Y); \rho \bigcup_{t \neq s} i^t(X) \mid \rho_{i^s}(X) \right).$$

This upper bound is weaker than Theorem 2 because it depends on the additional terms  $A_s$  and  $B_s$  which account for the degree of dependence between projections and can not be easily controlled. This can be seen as a confirmation that our metrics convey strictly more information than the unstructured DCI framework. We provide additional insights about the terms  $A_s$  and  $B_s$  in the supplementary material. We also provide an exact equality rather than two matching bounds in the case where  $n = 2$ , which is applicable to object-centric representations.

## 4. Permutation Invariant Affinity Scores

Crucial to our metric is the affinity matrix  $R = (R_{\hat{\tau}, \tau})$ , where  $R_{\hat{\tau}, \tau}$  measures the relative importance of latent  $z_{\hat{\tau}}$  in predicting factor  $v_{\tau}$ . To obtain these scores, prior work has focused either on regression feature importances or on mutual information between latents and factors (see the discussion of prior disentanglement metrics in the supplementary material). When attempting to adapt these techniques to object-centric latent representations, we encountered a domain-specific problem, caused by the non-deterministic ordering of the slots in the representation. Indeed, the image reconstruction is invariant to slot ordering. Neither mutual information nor traditional regression are able to accurately capture such a permutation invariance property. To address this problem, we used two complementary strategies. First, we developed an algorithm for obtaining permutation invariant feature importances, described in Section 4.1. Second, we divided our evaluation datasets into groups of images with similar factor values, which is described in Section 4.2.

### 4.1. Permutation invariant feature importances

A standard predictor is unable to capture invariance with respect to slot ordering. A theoretical possibility is to explore all the possible permutations in the evaluation dataset when fitting the regression. But this systematic exploration leads

to combinatorial explosion and is therefore untractable, as the best permutation of slots might be different for all evaluation samples. To address this problem, we developed an iterative algorithm for finding a good slot-permutation for all the evaluation samples (Algorithm 1). This algorithm can be seen as an EM-like approach. In the M-step, a standard predictor is fitted to the features with the current best slot permutations. In the E-step, the different inputs are permuted in order to obtain the minimal error for a fixed predictor. In Figure 3, we provide a visual inspection of the slot permutation learned for IODINE, showing that it manages to provide a consistent slot ordering across groups of similar inputs. The supplementary contains more detailed visualizations. In the supplementary, we provide an ablation study of Algorithm 1 (Table 3).

Developing algorithms that preserve permutation-invariance is no doubt a major challenge for the machine learning community: similar problematics appear in a variety of applications, ranging from speaker separation in the cocktail-party problem (Yu et al., 2017) to object detection losses (Carion et al., 2020). Algorithm 1 is to our knowledge the first algorithm that obtains permutation invariant feature importances, and we hope to it will applicable in other situations.

---

**Algorithm 1** Permutation-invariant feature importances

---

```

Input: Latent codes  $z^1, \dots, z^n$  and factor values
 $v^1, \dots, v^n$  for  $n$  input images
for  $i = 1$  to  $n_{\text{iters}}$  do
    # M STEP
    Fit predictor  $f_i$  to features  $z^1, \dots, z^n$  and targets
     $v^1, \dots, v^n$ .
    # E STEP
    for  $j = 1$  to  $n$  do
        #  $\pi$  ranges on all slot permutations
         $\pi_{\min} \leftarrow \arg \min \|v^j - f_i(\pi(z^j))\|_2$ 
         $z^j \leftarrow \pi_{\min}(z^j)$ 
    end for
    end for
    Fit  $f_{\text{final}}$  to features  $z^1, \dots, z^n$  and targets  $v^1, \dots, v^n$ .
    Obtain feature importances from  $f_{\text{final}}$ .

```

---

## 4.2. Local evaluation of disentanglement

A complementary strategy is to divide the evaluation datasets into groups of inputs with similar factor values. The underlying assumption is that the object-to-slot assignment should stay fixed for similar images. Experimentally, we observe this assumption does not always hold, but this method at least provides a good initialization for our iterative permutation-invariant feature importance algorithm. Moreover, it breaks the symmetry between factors, allowing for meaningful visualization of the projected latent space.

To obtain a global metric, we average the values across the different groups. The method for generating the evaluation dataset is summarized in Algorithm 2. Additional details such as hyperparameters are given in the supplementary.

---

**Algorithm 2** Generation of the evaluation dataset

---

```

for  $g = 1$  to  $n_{\text{groups}}$  do
    # Generate initial factor values for the group
    for  $f$  in factors do
        Sample initial value  $\text{initial}[f]$  for factor  $f$ 
    end for
    for  $i = 1$  to  $n_{\text{samples}}$  do
        # Sample factor values locally
        for  $f$  in factors do
            Sample value  $\text{image}_i[f]$  near  $\text{initial}[f]$ 
            Generate image  $i$  from factor values  $\text{image}_i$ 
        end for
    end for
end for

```

---

## 5. Experimental Evaluation

**Models** We compare three different architectures with public Pytorch implementations: MONet, GENESIS and IODINE, which we believe to be representative of object-centric representations. We evaluate two variants of MONet: the first one, denoted as "MONet (Engelcke)" follows (Engelcke et al., 2019) and uses the masks inferred by the attention network in the reconstruction. The second, simply denoted as MONet, uses the decoded mask, which is more faithful to the original design in (Burgess et al., 2019). For all models, we compare trainings with and without variational loss. The ablated models are denoted with (R).

**Datasets** We evaluate all models on CLEVR6 (Johnson et al., 2017) and Multi-dSprites (Matthey et al., 2017; Burgess et al., 2019), with the exception of IODINE that we restricted to Multi-dSprites for computational reasons.<sup>1</sup> These datasets are the most common benchmarks for learning object-centric latent representations. Both contain images generated compositionally, but they differ by the class of possible objects and background. Shapes in Multi-dSprites are purely two dimensional on a uniform background with variable color, while images in CLEVR6 are projections of 3D scenes on a unique gray background. We slightly modified the CLEVR6 dataset in order to ensure that all objects are visible in the cropped image. We give additional details about the generation in the supplementary.

Our **key experimental results** are as follows:

- The reliably good ARI scores obtained by most models

---

<sup>1</sup>(CLEVR6 requires a week on 8 V100 GPUs per training)

do not account for the high variation in representation quality measured by our disentanglement metric.

- We even observe evidences of negative correlation between ARI and representation quality, which can be harmful for the model selection process.
- This negative correlation also suggests that our metric addresses the dependence of ARI on sharp segmentation masks. In particular, IODINE achieves good object-level disentanglement despite its lower ARI.
- Our ablation experiment shows that visual object separation is mostly influenced by architectural inductive biases. However, auxiliary variational losses have a significant impact on representation quality.
- GENESIS separate encoding of masks overall seems beneficial to representation quality.

Table 1 contains our main experimental results. We give disentanglement and completeness values at both object-level (measuring object-separation between slots) and property-level (measuring disentanglement inside slots). We also display global informativeness and prior pixel-level segmentation metrics (ARI and mSC). Figure 2 shows a visualization of the different latent space projections on Multi-dSprites. Figure 3 shows the effect of Algorithm 1 on slot ordering. We provide detailed results in the supplementary.

**Pixel-level segmentation metrics** We obtain reliably high ARI and mSC values for all models (except IODINE on Multi-dSprites, which is consistent with measurements in (Greff et al., 2019)). We obtain slightly higher values than prior work for Multi-dSprites, and slightly lower for CLEVR6, which can be attributed to minor differences in the dataset generation process (see supplementary). The larger deviation of mSC is most likely due to the importance of small objects caused by its unweighted average. In the ablation study, we observe that models with pure reconstruction loss tend to get better pixel-level scores, supporting our claim that visual object separation is mostly influenced by architectural inductive biases rather than variational losses.

**Disentanglement criteria** Our disentanglement, completeness and informativeness metrics exhibit much higher variation, both between different runs of a given model and between models. MONet, GENESIS and IODINE can all achieve satisfying performance with the right configuration. At object-level, we observe that disentanglement and completeness match quite closely, but this is not the case at property-level. We attribute this to the asymmetry caused by the different number of factors and slot dimensions. (GENESIS has 80 dimensions per slot, the other representations are padded with zeros for fair comparison). Among the

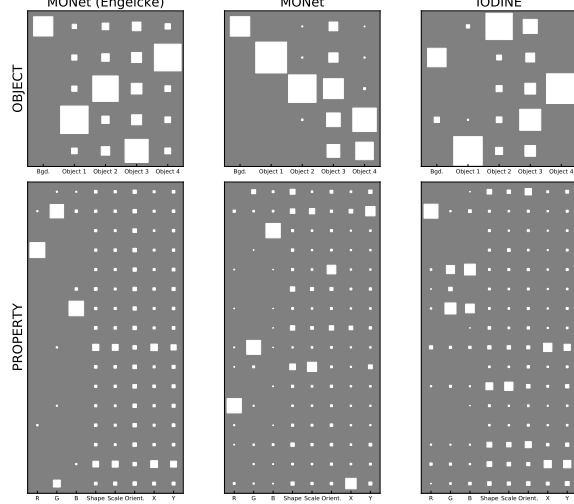


Figure 2. Projections of the affinity matrix on Multi-dSprites for IODINE and the two variants of MONet. (Hinton diagram)

considered models, GENESIS is the most reliable in obtaining good performance, which advocates for generalization of its separate mask encoding process. On Multi-dSprites, IODINE is able to match the object separation performance of MONet, despite its less stable training process resulting in an outlier. The ability of IODINE to obtain good object-level scores despite its lower ARI confirms that our metric reduced the dependence on sharp segmentation masks.

**Ablation study** Ablation of variational loss (marked as (R)) has a strong negative impact on disentanglement, completeness and informativeness. This is not surprising as the positive impact of variational losses is well-known in the case of unstructured latent representations (Eastwood & Williams, 2018; Locatello et al., 2019). However, the ablation improves ARI and mSC values. This negative correlation call into question the validity of prior model selection processes focused primarily on ARI. As a side note, the recent Slot Attention (Locatello et al., 2020) architecture does not even have a variational loss. In lights of our results, we believe that this is potentially harmful. Unfortunately, there is no complete Pytorch implementation available at the time of writing to verify this hypothesis. Finally, our results seem to suggest that visual object separation in all models is mostly influenced by architectural inductive biases.

**Variants of MONet** This negative correlation and its effect on model selection also appears when comparing variants of MONet. The choice of (Engelcke et al., 2019) to directly use masks generated by the attention network in the reconstruction was probably motivated by its faster convergence to visually satisfying results and its better seg-

Table 1. Comparison of the different models on Multi-dSprites and CLEVR6. We report mean and standard error over three random seeds. All values are in %. 100 is the best possible score and 0 the worst, except for the informativeness metric where 0 is best. Models denoted with (R) are trained with pure reconstruction loss.

MODEL	OBJECT-LEVEL		PROPERTY-LEVEL		INF. (↓)	ARI (↑)	MSC (↑)
	DIS. (↑)	COMP. (↑)	DIS. (↑)	COMP. (↑)			
MDSPR.	MONET (ENGELCKE)	52 ± 4	52 ± 4	39 ± 6	60 ± 5	45 ± 3	95 ± 1
	MONET (ENGELCKE) (R)	60 ± 4	60 ± 4	29 ± 3	52 ± 1	36 ± 2	<b>98 ± 0.1</b>
	MONET	75 ± 7	75 ± 7	59 ± 6	<b>74 ± 5</b>	26 ± 6	80 ± 4
	MONET (R)	69 ± 0.3	69 ± 0.2	35 ± 1	55 ± 1	32 ± 0.8	91 ± 0.2
	GENESIS	<b>90 ± 0.8</b>	<b>91 ± 0.6</b>	<b>72 ± 0.5</b>	60 ± 0.4	<b>24 ± 0.4</b>	85 ± 0
	GENESIS (R)	64 ± 3	65 ± 3	65 ± 1	42 ± 1	30 ± 0.5	96 ± 0.6
	IODINE	70 ± 9	72 ± 10	37 ± 5	62 ± 4	37 ± 6	80 ± 8
CLEVR6	IODINE (R)	35 ± 2	36 ± 1	17 ± 2	46 ± 1	61 ± 2	71 ± 3
	MONET (ENGELCKE)	<b>46 ± 5</b>	<b>48 ± 5</b>	22 ± 4	<b>51 ± 3</b>	55 ± 5	<b>93 ± 0.4</b>
	MONET (ENGELCKE) (R)	40 ± 9	41 ± 9	13 ± 5	44 ± 3	61 ± 8	<b>93 ± 0.4</b>
	MONET	<b>47 ± 6</b>	<b>48 ± 6</b>	21 ± 6	<b>50 ± 4</b>	55 ± 5	90 ± 2
	MONET (R)	40 ± 1	41 ± 0.2	13 ± 0.6	44 ± 0.1	60 ± 0.6	<b>92 ± 0.5</b>
	GENESIS	<b>50 ± 2</b>	<b>52 ± 2</b>	<b>47 ± 2</b>	39 ± 2	<b>47 ± 0.9</b>	91 ± 0.4
	GENESIS (R)	43 ± 1	45 ± 2	24 ± 2	21 ± 2	65 ± 1	92 ± 0.2

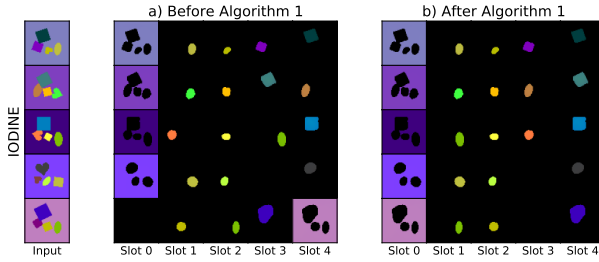


Figure 3. Visualization of the effect of Algorithm 1 on slot ordering for a group of similar inputs.

mentation metrics, which are particularly blatant on Multi-dSprites. However, this design choice decreases the pressure for accurate encoding of the segmentation mask in the latent representation, which has a negative impact captured by our metric. Our second version of MONet instead uses the reconstructed masks and addresses this issue.

## 6. Related work

**Structured disentanglement metrics** Most similar to our work is the slot compactness metric in (Racah & Chadar, 2020), also based on aggregation of feature importances to measure object separation of objects between slots. However, it is not generalized to arbitrary hierarchies, which makes it unable to evaluate internal slot representations. Besides, it does not handle the question of slot permutation invariance, which according to our experiments is essen-

tial to obtain meaningful results. Also related is (Esmaeili et al., 2019), where the authors develop a structured variational loss, with the goal of encouraging disentanglement at group-level. There is a high-level connection with our work, but they ultimately follow a different objective. It is worth noting that (Esmaeili et al., 2019) evaluate their structured variational loss with unstructured disentanglement metrics.

**Object-compositional generation** Object compositionality is also believed to be a promising inductive bias for purely generative models (van Steenkiste et al., 2018). Obtaining good latent representations and producing realistic samples are strongly connected: they both require to develop suitable decoder architectures. Very recent work has been focusing on integrating object compositionality into the GAN framework: Block-GAN (Nguyen-Phuoc et al., 2020), RELATE (Ehrhardt et al., 2020), GIRAFFE (Niemeyer & Geiger, 2020). The question of disentanglement is also present in this context of (Nguyen-Phuoc et al., 2019), but it remains a secondary objective.

## 7. Conclusion

We propose a novel method for evaluating disentanglement of structured latent representations. Our experimental evaluation shows that our framework addresses a number of issues with prior pixel-level image segmentation metrics. We hope that our metric will be helpful in future work about object-centric latent representations for hyper-parameter optimization, model selection and evaluation.

## Acknowledgements

This work was granted access to the HPC resources of IDRIS under the allocation 2020-AD011012138 made by GENCI. We would like to thank Frederik Benzing, Kalina Petrova, Asier Mujika, and Wouter Tonnon for helpful discussions. This work constitutes the public version of Raphaël Dang-Nhu's Master Thesis at ETH Zürich.

## References

Arbelaez, P., Maire, M., Fowlkes, C., and Malik, J. Contour detection and hierarchical image segmentation. *IEEE transactions on pattern analysis and machine intelligence*, 33(5):898–916, 2010.

Battaglia, P. W., Hamrick, J. B., Bapst, V., Sanchez-Gonzalez, A., Zambaldi, V., Malinowski, M., Tacchetti, A., Raposo, D., Santoro, A., Faulkner, R., et al. Relational inductive biases, deep learning, and graph networks. *arXiv preprint arXiv:1806.01261*, 2018.

Bengio, Y., Courville, A., and Vincent, P. Representation learning: A review and new perspectives. *IEEE transactions on pattern analysis and machine intelligence*, 35(8):1798–1828, 2013.

Brunton, S. L., Noack, B. R., and Koumoutsakos, P. Machine learning for fluid mechanics. *Annual Review of Fluid Mechanics*, 52:477–508, 2020.

Burgess, C. P., Matthey, L., Watters, N., Kabra, R., Higgins, I., Botvinick, M., and Lerchner, A. Monet: Unsupervised scene decomposition and representation. *arXiv preprint arXiv:1901.11390*, 2019.

Carion, N., Massa, F., Synnaeve, G., Usunier, N., Kirillov, A., and Zagoruyko, S. End-to-end object detection with transformers. *arXiv preprint arXiv:2005.12872*, 2020.

Chen, R. T., Li, X., Grosse, R. B., and Duvenaud, D. K. Isolating sources of disentanglement in variational autoencoders. In *Advances in Neural Information Processing Systems*, pp. 2610–2620, 2018.

Codd, E. F. A relational model of data for large shared data banks. In *Software pioneers*, pp. 263–294. Springer, 2002.

Cover, T. M. *Elements of information theory*. John Wiley & Sons, 1999.

Dang-Nhu, R. Plans: Robust program learning from neurally inferred specifications. *arXiv preprint arXiv:2006.03312*, 2020.

Dang-Nhu, R., Singh, G., Bielik, P., and Vechev, M. Adversarial attacks on probabilistic autoregressive forecasting models. *arXiv preprint arXiv:2003.03778*, 2020.

Dempster, A. P., Laird, N. M., and Rubin, D. B. Maximum likelihood from incomplete data via the em algorithm. *Journal of the Royal Statistical Society: Series B (Methodological)*, 39(1):1–22, 1977.

Eastwood, C. and Williams, C. K. A framework for the quantitative evaluation of disentangled representations. 2018.

Ehrhardt, S., Groth, O., Monszpart, A., Engelcke, M., Posner, I., Mitra, N., and Vedaldi, A. Relate: Physically plausible multi-object scene synthesis using structured latent spaces. *arXiv preprint arXiv:2007.01272*, 2020.

Engelcke, M., Kosiorek, A. R., Jones, O. P., and Posner, I. Genesis: Generative scene inference and sampling with object-centric latent representations. *arXiv preprint arXiv:1907.13052*, 2019.

Esmaeili, B., Wu, H., Jain, S., Bozkurt, A., Siddharth, N., Paige, B., Brooks, D. H., Dy, J., and Meent, J.-W. Structured disentangled representations. In *The 22nd International Conference on Artificial Intelligence and Statistics*, pp. 2525–2534. PMLR, 2019.

Greff, K., Rasmus, A., Berglund, M., Hao, T., Valpola, H., and Schmidhuber, J. Tagger: Deep unsupervised perceptual grouping. In *Advances in Neural Information Processing Systems*, pp. 4484–4492, 2016.

Greff, K., Van Steenkiste, S., and Schmidhuber, J. Neural expectation maximization. In *Advances in Neural Information Processing Systems*, pp. 6691–6701, 2017.

Greff, K., Kaufman, R. L., Kabra, R., Watters, N., Burgess, C., Zoran, D., Matthey, L., Botvinick, M., and Lerchner, A. Multi-object representation learning with iterative variational inference. *arXiv preprint arXiv:1903.00450*, 2019.

Higgins, I., Matthey, L., Pal, A., Burgess, C., Glorot, X., Botvinick, M., Mohamed, S., and Lerchner, A. betavae: Learning basic visual concepts with a constrained variational framework. 2016.

Johnson, J., Hariharan, B., van der Maaten, L., Fei-Fei, L., Lawrence Zitnick, C., and Girshick, R. Clevr: A diagnostic dataset for compositional language and elementary visual reasoning. In *Proceedings of the IEEE Conference on Computer Vision and Pattern Recognition*, pp. 2901–2910, 2017.

Kim, H. and Mnih, A. Disentangling by factorising. *arXiv preprint arXiv:1802.05983*, 2018.

Kumar, A., Sattigeri, P., and Balakrishnan, A. Variational inference of disentangled latent concepts from unlabeled observations. *arXiv preprint arXiv:1711.00848*, 2017.

Lake, B. M., Ullman, T. D., Tenenbaum, J. B., and Gershman, S. J. Building machines that learn and think like people. *Behavioral and brain sciences*, 40, 2017.

Li, N., Fisher, R., et al. Learning object-centric representations of multi-object scenes from multiple views. *Advances in Neural Information Processing Systems*, 33, 2020.

Lin, Z., Wu, Y.-F., Peri, S. V., Sun, W., Singh, G., Deng, F., Jiang, J., and Ahn, S. Space: Unsupervised object-oriented scene representation via spatial attention and decomposition. *arXiv preprint arXiv:2001.02407*, 2020.

Locatello, F., Bauer, S., Lucic, M., Raetsch, G., Gelly, S., Schölkopf, B., and Bachem, O. Challenging common assumptions in the unsupervised learning of disentangled representations. In *international conference on machine learning*, pp. 4114–4124, 2019.

Locatello, F., Weissenborn, D., Unterthiner, T., Mahendran, A., Heigold, G., Uszkoreit, J., Dosovitskiy, A., and Kipf, T. Object-centric learning with slot attention. *Advances in Neural Information Processing Systems*, 33, 2020.

Matthey, L., Higgins, I., Hassabis, D., and Lerchner, A. dsprites: Disentanglement testing sprites dataset. *URL https://github.com/deepmind/dsprites-dataset/* [Accessed on: 2018-05-08], 2017.

Meier, F., Dang-Nhu, R., and Steger, A. Adaptive tuning curve widths improve sample efficient learning. *Frontiers in computational neuroscience*, 14:12, 2020.

Nguyen-Phuoc, T., Li, C., Theis, L., Richardt, C., and Yang, Y.-L. Hologan: Unsupervised learning of 3d representations from natural images. In *Proceedings of the IEEE International Conference on Computer Vision*, pp. 7588–7597, 2019.

Nguyen-Phuoc, T., Richardt, C., Mai, L., Yang, Y.-L., and Mitra, N. Blockgan: Learning 3d object-aware scene representations from unlabelled images. *arXiv preprint arXiv:2002.08988*, 2020.

Niemeyer, M. and Geiger, A. Giraffe: Representing scenes as compositional generative neural feature fields. *arXiv preprint arXiv:2011.12100*, 2020.

Racah, E. and Chandar, S. Slot contrastive networks: A contrastive approach for representing objects. *arXiv preprint arXiv:2007.09294*, 2020.

Rand, W. M. Objective criteria for the evaluation of clustering methods. *Journal of the American Statistical association*, 66(336):846–850, 1971.

Rezende, D. J. and Viola, F. Generalized elbo with constrained optimization, geco. In *Workshop on Bayesian Deep Learning, NeurIPS*, 2018.

Ridgeway, K. and Mozer, M. C. Learning deep disentangled embeddings with the f-statistic loss. In *Advances in Neural Information Processing Systems*, pp. 185–194, 2018.

Spelke, E. S., Breinlinger, K., Macomber, J., and Jacobson, K. Origins of knowledge. *Psychological review*, 99(4):605, 1992.

Van Steenkiste, S., Chang, M., Greff, K., and Schmidhuber, J. Relational neural expectation maximization: Unsupervised discovery of objects and their interactions. *arXiv preprint arXiv:1802.10353*, 2018.

van Steenkiste, S., Kurach, K., and Gelly, S. A case for object compositionality in deep generative models of images. *arXiv preprint arXiv:1810.10340*, 2018.

Wang, T., Liao, R., Ba, J., and Fidler, S. Nervenet: Learning structured policy with graph neural networks. In *International Conference on Learning Representations*, 2018.

Watters, N., Matthey, L., Bosnjak, M., Burgess, C. P., and Lerchner, A. Cobra: Data-efficient model-based rl through unsupervised object discovery and curiosity-driven exploration. *arXiv preprint arXiv:1905.09275*, 2019.

Yu, D., Kolbæk, M., Tan, Z.-H., and Jensen, J. Permutation invariant training of deep models for speaker-independent multi-talker speech separation. In *2017 IEEE International Conference on Acoustics, Speech and Signal Processing (ICASSP)*, pp. 241–245. IEEE, 2017.

## A. Additional Related Work

### A.1. Object-centric representation learning

Many models have been developed to perform unsupervised perceptual grouping and learn compositional representations. A first line of work (TAGGER (Greff et al., 2016), NEM (Greff et al., 2017), R-NEM (Van Steenkiste et al., 2018)) has focused on adapting traditional Expectation Maximization (EM) (Dempster et al., 1977) methods for data clustering to a differentiable neural setting. Nonetheless, despite strong theoretical foundations, these models do not scale to more complex multi-object datasets such as Multi-dSprites (Burgess et al., 2019) and CLEVR (Johnson et al., 2017). More recent efforts (MONet (Burgess et al., 2019), IODINE (Greff et al., 2019), GENESIS (Engelcke et al., 2019)), Slot Attention (Locatello et al., 2020)) have focused on application to these datasets.

These architectures differ by how exactly they segment the image between the different slots of the representation. MONet is based on a recurrent attention network that repeatedly separates parts of the image until it is totally decomposed. GENESIS was designed to address a key limitation of MONet, namely that it does not learn a latent representation for the segmentation, which prevents principled sampling of novel scenes. With GENESIS, segmentation masks are separately encoded, and an autoregressive prior on the mask latents is enforced. IODINE uses a different strategy building upon the framework of iterative amortized inference, where an initial arbitrary guess for the posterior is progressively refined. However, this iterative process is very computationally expensive. Slot Attention, as its name indicates, introduces an attention based iterative encoder that is much more computationally efficient than Iodine. The SPACE model (Lin et al., 2020) combines the strength of spatial attention with scene mixture models to further improve applicability. Finally, MulMON (Li et al., 2020) extends object-centric representations to a setting with multi-view supervision.

### A.2. Traditional disentanglement metrics

Several metrics have been developed to evaluate the quality of learned representations and allow comparison between models. From a high-level perspective, we identify two main categories:

**Classifier-based metrics** The first group of metrics is based on fixing the value of a factor of variation and generating several samples sharing this value. Intuitively, if the factors of variation are satisfactorily disentangled in the representation, it should be possible to predict which factor was fixed from the different latents. Inside this category, the metric differ in how they exactly identify the factor. Be-

taVAE (Higgins et al., 2016) uses a linear classifier to predict the factor index, while FactorVAE uses majority vote and takes the empirical variances as input, with the goal of addressing several robustness issues. Despite these implementation differences, Locatello et al. (Locatello et al., 2019) have empirically observed that both metrics are strongly correlated across a wide range of tasks and models.

**Affinity-based metrics** The second category of metrics is based on measuring the affinity between each factor of variation and each latent variable, and evaluating how close these are to a one-to-one mapping between factors and variables. Different ways of quantifying affinity have been proposed: the Mutual Information Gap (Chen et al., 2018) and Modularity (Ridgeway & Mozer, 2018) measure mutual information between factors and variables. The SAP score (Kumar et al., 2017) leverages the linear coefficient of determination  $R^2$  obtained when regressing the factor from the latent. Finally, the DCI metric (Eastwood & Williams, 2018) is based on measuring regression feature importance, using either Lasso or random forests. These metrics also differ on how they exactly assess the separation of factors in the latent representation. The Mutual Information Gap and the SAP score measure the gap between the two most relevant variables for a factor. Modularity alternatively suggests to quantify the distance to an ideal affinity template. Finally, the DCI metric uses the entropy of the normalized feature importances as an indicator of entanglement.

In developing our metric, we have chosen to privilege the affinity-based approach for two reasons. First, it does not require the ability to fix one factor while generating samples, contrary to BetaVAE and FactorVAE. Second, the notion of affinity generalizes in a very flexible way to group of factors and latent variables: it is sufficient to sum the scores of all pairs of factors and variables in the groups. We use regression feature importance as a way of measuring affinity. Moreover, we privilege the entropy measure of separation over affinity-gap methods. Indeed, we believe that entropy captures more information about the repartition of information as it takes into account all coefficients rather than just the top two.

## B. Proofs And Additional Theoretical Results

### B.1. Background in information theory

The description of our metric leverages concepts originating from the field of information-theory (Cover, 1999). In this section, we recall some central definitions and results that we will use in the rest of the manuscript. In all of the following,  $X$ ,  $Y$  and  $Z$  denote three discrete random variables defined on a common probability space. We denote  $x_1, \dots, x_l$  (resp  $y_1, \dots, y_m$  and  $z_1, \dots, z_n$ ) the potential

outcomes of  $X$  (resp.  $Y$  and  $Z$ ).  $K$  is a positive real number. For brevity reasons, we denote  $\mathbb{P}[x_i]$  for  $\mathbb{P}[X = x_i]$ , and similarly for  $Y$  and  $Z$  and the joint random variables.

**Definition 3.** *The entropy of  $X$  in base  $K$  quantifies the amount of uncertainty in the potential outcomes of  $X$ . It is defined as*

$$H_K(X) = -\mathbb{E}[\log_K(\mathbb{P}(X))] = -\sum_{i=1}^l \mathbb{P}[x_i] \log_K(\mathbb{P}[x_i]).$$

**Definition 4.** *The conditional entropy of  $Y$  given  $X$  in base  $K$  quantifies the amount of information needed to describe the outcome of  $Y$  given that the value of  $X$  is known. It is defined as*

$$H_K(Y|X) = -\sum_{i,j} \mathbb{P}[x_i, y_j] \log_K(\mathbb{P}[y_j|x_i]).$$

**Definition 5.** *The mutual information of  $X$  and  $Y$  in base  $K$  is a measure of the amount of information obtained about one of the two variables by observing the other. It is defined as*

$$I_K(X; Y) = \sum_{i,j} \mathbb{P}[x_i, y_j] \log_K \left( \frac{\mathbb{P}[x_i, y_j]}{\mathbb{P}[x_i] \cdot \mathbb{P}[y_j]} \right).$$

**Definition 6.** *The conditional mutual information  $I_K(X; Y|Z)$  is, in base  $K$ , the expected value of the mutual information of  $X$  and  $Y$  conditioned on the value of  $Z$ . Formally,*

$$I_K(X; Y|Z) = \sum_{i,j,k} \mathbb{P}[x_i, y_j, z_k] \log_K \left( \frac{\mathbb{P}[x_i, y_j, z_k]}{\mathbb{P}[x_i|z_k] \mathbb{P}[y_j|z_k]} \right)$$

The following Lemmas are standard results of information theory. As these are well-known, we did not provide a proof here and we refer to textbooks such as (Cover, 1999).

**Lemma 1** (Change of base). *Let  $K^1$  be a positive real number. The change of base formula for entropy is*

$$H_{K^1}(X) = \frac{H_K(X)}{\log_{K^1} K}.$$

Similarly, we have for conditional entropy that

$$H_{K^1}(Y|X) = \frac{H_K(Y|X)}{\log_{K^1} K}.$$

**Lemma 2** (Subadditivity of entropy). *Let  $X_1, \dots, X_n$  be  $n$  arbitrary discrete random variables. We have*

$$H_K(X_1, \dots, X_n) \leq \sum_{i=1}^n H_K(X_i).$$

The same holds for conditional entropy, i.e.

$$H_K(X_1, \dots, X_n|Y) \leq \sum_{i=1}^n H_K(X_i|Y).$$

**Lemma 3** (Nonnegativity of mutual information). *The following holds*

$$H_K(X) - H_K(X|Y) = I_K(X; Y) \geq 0.$$

Conditioned on a third variable, this generalizes to

$$H_K(X|Z) - H_K(X|Y, Z) = I_K(X; Y|Z) \geq 0.$$

**Lemma 4** (Relation of joint entropy to individual entropies). *Let  $X_1, \dots, X_n$  be  $n$  arbitrary discrete random variables. We have*

$$H_K(X_1, \dots, X_n) \geq \max_{i=1}^n H_K(X_i).$$

The same holds for conditional entropy, i.e.

$$H_K(X_1, \dots, X_n|Y) \geq \max_{i=1}^n H_K(X_i|Y).$$

**Lemma 5** (Joint conditional entropy). *The following holds*

$$H_K(X, Y|Z) = H_K(X|Z) + H_K(Y|Z) - I_K(X; Y|Z).$$

## B.2. Proofs

**Theorem 1.** *With the total projection  $i = \{1, \dots, n\}$ , our metric captures the disentanglement and completeness metrics of the DCI framework (Eastwood & Williams, 2018).*

*Proof.* We will only present the proof for the completeness metric, as the situation for the disentanglement metric is exactly symmetric, when switching  $X$  and  $Y$  and rows and columns. With the total projection  $i = \{1, \dots, n\}$ , we have  $\rho_i(Y) = Y$ ,  $\rho_i(X) = X$ ,  $U = |\rho_i(\hat{\mathcal{T}})| = |\hat{\mathcal{T}}| = L$  and  $V = |\rho_i(\mathcal{T})| = |\mathcal{T}| = F$ .

Therefore, completeness with respect to the total projection is defined as

$$C(i) = 1 - H_L(X|Y).$$

According to Definition 4, we have

$$\begin{aligned} & H_L(X|Y) \\ &= - \sum_{\tau \in \mathcal{T}, \hat{\tau} \in \hat{\mathcal{T}}} \mathbb{P}[X = \hat{\tau}, Y = \tau] \log_L(\mathbb{P}[X = \hat{\tau}|Y = \tau]) \\ &= - \sum_{\tau \in \mathcal{T}} \mathbb{P}[Y = \tau] \sum_{\hat{\tau} \in \hat{\mathcal{T}}} \mathbb{P}[\hat{\tau}|\tau] \log_L(\mathbb{P}[\hat{\tau}|\tau]). \end{aligned}$$

Now, let us observe that the conditional probability  $\mathbb{P}[\hat{\tau}|\tau]$  is exactly the term  $\tilde{P}_{\hat{\tau}, \tau}$  of the DCI framework that denotes the "probability" of latent  $\hat{\tau}$  being important to predict factor  $\tau$ . Consequently, the conditional entropy can be rewritten as follows

$$\begin{aligned} H_L(X|Y) &= - \sum_{\tau \in \mathcal{T}} \mathbb{P}[Y = \tau] \sum_{\hat{\tau} \in \hat{\mathcal{T}}} \tilde{P}_{\hat{\tau}, \tau} \log_L(\tilde{P}_{\hat{\tau}, \tau}) \\ &= \sum_{\tau \in \mathcal{T}} \mathbb{P}[Y = \tau] H_L(\tilde{P}_{\cdot, \tau}). \end{aligned}$$

This yields

$$\begin{aligned} C(i) &= 1 - H_L(X|Y) \\ &= \sum_{\tau \in \mathcal{T}} \mathbb{P}[Y = \tau] (1 - H_L(\tilde{P}_{\cdot, \tau})) \\ &= \sum_{\tau \in \mathcal{T}} \mathbb{P}[Y = \tau] C_{\tau}. \end{aligned}$$

We observe that  $C_{\tau} = 1 - H_L(\tilde{P}_{\cdot, \tau})$  is exactly the completeness score in capturing factor  $\tau$  defined in the DCI framework. Besides,  $\mathbb{P}[Y = \tau]$  can be rewritten as

$$\begin{aligned} \mathbb{P}[Y = \tau] &= \sum_{\hat{\tau} \in \hat{\mathcal{T}}} \mathbb{P}[Y = \tau, X = \hat{\tau}] \\ &= \frac{\sum_{\hat{\tau} \in \hat{\mathcal{T}}} R_{\hat{\tau}, \tau}}{\sum_{i \in \hat{\mathcal{T}}, j \in \mathcal{T}} R_{i, j}}, \end{aligned}$$

which is exactly the relative generative factor importance used by Eastwood and Williams to construct a weighted average expressing overall completeness. This indicates that our probabilistic view of the affinity matrix and metric naturally captures all components of the DCI framework, including the final weighted average step.  $\square$

**Theorem 2** (Lower bound). *Consider  $k$  disjunct projections  $i^1, \dots, i^k$  of the relations. Let us suppose that  $i^1, \dots, i^k$  have respectively  $L^1, \dots, L^k$  groups of latents and  $F^1, \dots, F^k$  groups of factors. Moreover, assume that the joint projection  $i = \bigcup_{s=1}^k i^s$  has  $L$  groups of latents and  $F$  groups of factors. The following lower bound for the joint completeness holds*

$$1 - k + \sum_{s=1}^k C(i^s) \leq 1 - \sum_{s=1}^k \frac{1 - C(i^s)}{\log_{L^s}(L)} \leq C \left( \bigcup_{s=1}^k i^s \right).$$

Similarly, we have for the disentanglement metric

$$1 - k + \sum_{s=1}^k D(i^s) \leq 1 - \sum_{s=1}^k \frac{1 - D(i^s)}{\log_{F^s}(F)} \leq D \left( \bigcup_{s=1}^k i^s \right).$$

*Proof.* We only detail the proof for the completeness metric since both cases are exactly symmetric.  $C(i)$  is defined as follows

$$C(i) = 1 - H_L(\rho_i(X) | \rho_i(Y)).$$

Now, let us observe that the joint projection  $\rho_i$  and the concatenation of the different projections  $\prod_{s=1}^k \rho_{i^s}$  are similar up to the permutation of the dimensions that originates from sorting the merged index sequences. This permutation has no influence on the conditional entropy since it is defined as a joint expectation on  $\hat{\mathcal{T}} \times \mathcal{T}$ . Therefore we have that

$$C(i) = 1 - H_L \left( \prod_{s=1}^k \rho_{i^s}(X) \mid \prod_{t=1}^k \rho_{i^t}(Y) \right). \quad (1)$$

According to Lemma 2, we have the following inequality for the joint conditional entropy

$$\begin{aligned} H_L \left( \prod_{s=1}^k \rho_{i^s}(X) \mid \prod_{t=1}^k \rho_{i^t}(Y) \right) \\ \leq \sum_{s=1}^k H_L \left( \rho_{i^s}(X) \mid \prod_{t=1}^k \rho_{i^t}(Y) \right). \end{aligned}$$

According to Lemma 3, we also know that

$$H_L \left( \rho_{i^s}(X) \mid \prod_{t=1}^k \rho_{i^t}(Y) \right) \leq H_L(\rho_{i^s}(X) | \rho_{i^s}(Y)).$$

Applying Lemma 1 to change base, we obtain

$$\begin{aligned} H_L(\rho_{i^s}(X) | \rho_{i^s}(Y)) &= \frac{H_{L^s}(\rho_{i^s}(X) | \rho_{i^s}(Y))}{\log_{L^s}(L)} \\ &= \frac{1 - C(i^s)}{\log_{L^s}(L)}. \end{aligned}$$

Together with Equation (1), this yields

$$1 - \sum_{s=1}^k \frac{1 - C(i^s)}{\log_{L^s}(L)} \leq C \left( \bigcup_{s=1}^k i^s \right).$$

Since  $\log_{L^s}(L) \geq 1$  and  $1 - C(i^s) \geq 0$ , we finally get

$$1 - k + \sum_{s=1}^k C(i^s) \leq 1 - \sum_{s=1}^k \frac{1 - C(i^s)}{\log_{L^s}(L)},$$

which concludes the proof.  $\square$

**Theorem 3** (Upper bound). *Consider  $k$  disjunct projections  $i^1, \dots, i^k$  of the relations. Let us suppose that  $i^1, \dots, i^k$  have respectively  $L^1, \dots, L^k$  groups of latents and  $F^1, \dots, F^k$  groups of factors. Moreover, assume that the joint projection  $i = \bigcup_{s=1}^k i^s$  has  $L$  groups of latents and  $F$  groups of factors. The following upper bound for the completeness metric holds*

$$C \left( \bigcup_{s=1}^k i^s \right) \leq 1 - \max_{1 \leq s \leq k} \left( \frac{1 - C(i^s)}{\log_{L^s} L} - A_s \right),$$

where

$$A_s = I_L \left( \rho_{i^s}(X); \rho_{\bigcup_{t \neq s} i^t}(Y) \mid \rho_{i^s}(Y) \right).$$

Similarly, we have for the disentanglement metric that

$$D \left( \bigcup_{s=1}^k i^s \right) \leq 1 - \max_{1 \leq s \leq k} \left( \frac{1 - D(i^s)}{\log_{F^s} F} - B_s \right).$$

where

$$B_s = I_F \left( \rho_{i^s}(Y); \rho_{\bigcup_{t \neq s} i^t}(X) \mid \rho_{i^s}(X) \right).$$

*Proof.* We only prove the bound for the completeness metric, as the case of disentanglement is exactly symmetric.  $C(i)$  is defined as follows

$$C(i) = 1 - H_L(\rho_i(X) | \rho_i(Y)).$$

Similar to the previous proof, we observe that the joint projection  $\rho_i$  and the concatenation of the different projections  $\prod_{s=1}^k \rho_{i^s}$  are similar up to the permutation of the dimensions that originates from sorting the merged index sequences. This permutation has no influence on the conditional entropy since it is defined as a joint expectation on  $\hat{\mathcal{T}} \times \mathcal{T}$ . Therefore we have that

$$C(i) = 1 - H_L\left(\prod_{s=1}^k \rho_{i^s}(X) | \prod_{t=1}^k \rho_{i^t}(Y)\right). \quad (2)$$

According to Lemma 4, we have the following inequality for the joint conditional entropy

$$\begin{aligned} & \max_{s=1}^k H_L\left(\rho_{i^s}(X) | \prod_{t=1}^k \rho_{i^t}(Y)\right) \\ & \leq H_L\left(\prod_{s=1}^k \rho_{i^s}(X) | \prod_{t=1}^k \rho_{i^t}(Y)\right) \end{aligned}$$

According to Lemma 3, we also know that

$$H_L\left(\rho_{i^s}(X) | \prod_{t=1}^k \rho_{i^t}(Y)\right) = H_L(\rho_{i^s}(X) | \rho_{i^s}(Y)) - A_s,$$

where

$$A_s = I_L\left(\rho_{i^s}(X); \rho_{\bigcup_{t \neq s} i^t}(Y) | \rho_{i^s}(Y)\right).$$

Applying Lemma 1 to change base, we obtain

$$H_L\left(\rho_{i^s}(X) | \prod_{t=1}^k \rho_{i^t}(Y)\right) = \frac{1 - C(i^s)}{\log_{L^s} L} - A_s.$$

Together with Equation (2), this yields

$$C(i) \leq 1 - \max_{1 \leq s \leq k} \left( \frac{1 - C(i^s)}{\log_{L^s} L} - A_s \right).$$

□

### B.3. Interpretation of the upper bound

The goal of Theorem 3 is to use the individual projections to obtain an upper bound for the joint disentanglement (resp. completeness). Intuitively, the meaning of the bound

$$C(i) \leq 1 - \max_{1 \leq s \leq k} \left( \frac{1 - C(i^s)}{\log_{L^s} L} - A_s \right).$$

is that the joint completeness can not be better than any of the individual completeness. However, this bound is weaker than Theorem 2 because of two main restrictions. First, it is harder to get rid of the  $\log_{L^s}(L)$  term as  $L$  is greater than  $L^s$ . One possibility is to notice that  $L \leq L^1 \times \dots \times L^k$ . If we make the additional assumption that  $L^1 \sim \dots \sim L^k$ , then we obtain  $\log_{L^s}(L) \leq k$ , which gives us

$$C(i) \leq 1 - \frac{1}{k} + \min_{1 \leq s \leq k} \left( \frac{C(i^s)}{k} + A_s \right).$$

This first assumption can be considered reasonable. But more importantly, we notice an additional interaction term  $A_s$  in the minimum that is based on mutual information between the different projections. This term can not be removed as it is non-negative. The intuition for this conditional mutual information is that it measures the dependence of the different projections. It is 0 exactly when  $\rho_{i^s}(X)$  and  $\rho_{\bigcup_{t \neq s} i^t}(Y)$  are independent conditioned on  $\rho_{i^s}(Y)$ . Assuming that this is case, we obtain the simplest inequality

$$C(i) \leq 1 - \frac{1}{k} + \min_{1 \leq s \leq k} \frac{C(i^s)}{k}.$$

However, there is absolutely no guarantee that this assumption is valid.

### B.4. Additional results

In the following, we study the specific case where there are only two levels of hierarchy ( $k = 2$ ). In this case, we can actually derive an exact formula rather two matching bounds.

**Theorem 4** (Case  $k = 2$ ). *Consider 2 disjunct projections  $i^1$  and  $i^2$ , with respectively  $L^1$  and  $L^2$  groups of latents, and  $F^1, F^2$  groups of factors. Assume that the joint projection  $i = i^1 \cup i^2$  has  $L$  groups of latents and  $F$  groups of factors. For the completeness metric, the following identity holds*

$$\begin{aligned} C(i) = & 1 - \frac{1 - C(i^1)}{\log_{L^1}(L)} - \frac{1 - C(i^2)}{\log_{L^2}(L)} \\ & + I_L(\rho_{i^1}(X); \rho_{i^1}(Y) | \rho_{i^2}(Y)) \\ & + I_L(\rho_{i^2}(X); \rho_{i^2}(Y) | \rho_{i^1}(Y)) \\ & + I_L(\rho_{i^1}(X); \rho_{i^2}(X) | \rho_{i^1}(Y), \rho_{i^2}(Y)). \end{aligned}$$

In a symmetric way, for the disentanglement metric,

$$\begin{aligned} D(i) = & 1 - \frac{1 - D(i^1)}{\log_{F^1}(F)} - \frac{1 - D(i^2)}{\log_{F^2}(F)} \\ & + I_F(\rho_{i^1}(Y); \rho_{i^1}(X) | \rho_{i^2}(X)) \\ & + I_F(\rho_{i^2}(Y); \rho_{i^2}(X) | \rho_{i^1}(X)) \\ & + I_F(\rho_i(Y); \rho_{i^2}(Y) | \rho_{i^1}(X), \rho_{i^2}(X)). \end{aligned}$$

*Proof.* Again, we only prove the result for the completeness metric as disentanglement is exactly symmetric. In the case

where  $k = 2$ , the joint completeness is defined as follows

$$\begin{aligned} C(i) &= 1 - H_L(\rho_i(X) | \rho_i(Y)) \\ &= 1 - H_L(\rho_{i^1}(X), \rho_{i^2}(X) | \rho_{i^1}(Y), \rho_{i^2}(Y)). \end{aligned}$$

With Lemma 5, we can rewrite this last expression as

$$\begin{aligned} C(i) &= 1 - H_L(\rho_{i^1}(X) | \rho_{i^1}(Y), \rho_{i^2}(Y)) \\ &\quad - H_L(\rho_{i^2}(X) | \rho_{i^1}(Y), \rho_{i^2}(Y)) \\ &\quad + I_L(\rho_{i^1}(X); \rho_{i^2}(X) | \rho_{i^1}(Y), \rho_{i^2}(Y)). \end{aligned}$$

Applying Lemma 3 twice, we obtain

$$\begin{aligned} &H_L(\rho_{i^1}(X) | \rho_{i^1}(Y), \rho_{i^2}(Y)) \\ &= H_L(\rho_{i^1}(X) | \rho_{i^1}(Y)) \\ &\quad - I_L(\rho_{i^1}(X); \rho_{i^1}(Y) | \rho_{i^2}(Y), \rho_{i^2}(Y)), \end{aligned}$$

and

$$\begin{aligned} &H_L(\rho_{i^2}(X) | \rho_{i^1}(Y), \rho_{i^2}(Y)) \\ &= H_L(\rho_{i^2}(X) | \rho_{i^2}(Y)) \\ &\quad - I_L(\rho_{i^2}(X); \rho_{i^2}(Y) | \rho_{i^1}(Y), \rho_{i^2}(Y)), \end{aligned}$$

Using Lemma 1 to change base for the two conditional entropies gives us the final equation

$$\begin{aligned} C(i) &= 1 - \frac{1 - C(i^1)}{\log_{L^1}(L)} - \frac{1 - C(i^2)}{\log_{L^2}(L)} \\ &\quad + I_L(\rho_{i^1}(X); \rho_{i^1}(Y) | \rho_{i^2}(Y)) \\ &\quad + I_L(\rho_{i^2}(X); \rho_{i^2}(Y) | \rho_{i^1}(Y)) + \\ &\quad + I_L(\rho_{i^1}(X); \rho_{i^2}(X) | \rho_{i^1}(Y), \rho_{i^2}(Y)), \end{aligned}$$

which concludes the proof.  $\square$

## C. Additional Experimental Results

### C.1. Disentanglement of intrinsic and extrinsic object properties

Our metric can be extended to more than two levels of hierarchy in the representation. The GENESIS architecture offers a good opportunity to experimentally demonstrate this claim. Indeed, each slot has an additional division between the mask and component latent. We quantify how much this separates the encoding of intrinsic and extrinsic object properties. Intuitively, intrinsic properties (such as shape and color) are related to the nature of the object, whereas extrinsic properties (such as position and orientation) are contextual to the scene. Table 6 indicated whether each of the considered factors is intrinsic or extrinsic. The question of whether to consider object size as intrinsic can be debated, however this does not change the observations of this section.

In Table 2, we show the projection of affinity matrix along this hierarchy level for a GENESIS trained model. We

Table 2. Projection of the affinity matrix along a third hierarchy level for a GENESIS model trained on Multi-dSprites.

		EXTRINSIC	INTRINSIC
MDSPR.	MASK LATENT	0.2	0.32
	COMPONENT LATENT	0	0.48

observe that extrinsic properties are successfully captured by the mask latent. However, intrinsic properties are not satisfactorily separated, which results in poor completeness and disentanglement for this projection. In our opinion, this observation points to the fundamental limitation of the segmentation mask approach for object-centric generative models. Indeed, the mask latent captures simultaneously extrinsic properties such as position and intrinsic properties such as object shape. We believe that recent architectures (Nguyen-Phuoc et al., 2020; Ehrhardt et al., 2020) performing object composition in 3D scene space are more adapted to disentanglement of intrinsic and extrinsic object properties.

### C.2. Visualization of the permutation inferred by our feature importance algorithm

In this Section, we inspect the slot ordering inferred by Algorithm 1, by visualizing the masked reconstruction for each slot. Note that Algorithm 1 does not make use of these reconstructions. In Figures 4, 5 and 6 we compare slot ordering before (on the left) and after (on the right) applying the algorithm, for two groups of similar images (generated following Algorithm 2). We include all the considered architectures, trained on Multi-dSprites with variational loss.

On the left, we observe that the slot ordering inferred by the models is not consistent across similar images. This effect is particularly visible for IODINE, despite the fact that we set the model internal noise to a deterministic value (following observations in (Greff et al., 2019)). The background slot is not even deterministic. This unpredictable ordering is extremely detrimental to the accuracy of our metric. Applying our metric to IODINE with this initial ordering yielded extremely poor values which do not do justice to the good representation learned by this model.

On the right, we see that Algorithm 1 successfully learns a consistent slot ordering, and puts matching objects at the same position. We notice almost perfect alignment, except for some failure cases with IODINE, where the background slot is switched with a missing object. We are uncertain as to the reasons for this failure, but it has limited impact on final performance as we remove the background factors in the object-level projection of the affinity matrix.

### C.3. Visualizations of the latent space

In Figures 7 and 8, we show visualizations of the projected latent space for the different architectures (trained with variational loss) for a group of inputs in both evaluation datasets. The qualitative inspection of the object-level projection is consistent with the numerical comparison: GENESIS is visually more disentangled, while MONet and IODINE achieve inferior but still satisfying disentanglement. On Multi-dSprites, the under-performance of the MONet variant from (Engelcke et al., 2019) is also visible. On Multi-dSprites, we observe that the GENESIS background slot also contains information about all objects. This is not surprising as the background mask is in some sense a negative of the different object masks. However, this phenomenon is less marked with other architectures. We think that the specific mask encoding of GENESIS somehow strengthens this duplication of information between background and object slot. Note that this does not harm performance as we removed the background slot in the final metric. We believe that this post-processing is fair because of the expected duplication effect described above.

Qualitative comparison of the property-level projections is harder due to the higher number of dimensions. Still, some observations can be made. Among object properties, color consistently obtain the best separation in the representation. On the GENESIS model, we also notice a clear separation between the last 16 dimensions that correspond to the component latent and the rest of the slot. Color is almost exclusively encoded by the component latent.

### C.4. Decomposition of the informativeness and completeness per factor

In Table 4, we decompose informativeness of the different models per property. Note that the completeness results do not necessarily average to the global object-level completeness as our metric involves a weighted average. On Multi-dSprites, we observe that the superior results of GENESIS mostly comes from the group of extrinsic factors that are related to the segmentation mask. This would support the hypothesis that the innovative mask encoding of GENESIS is at least partly responsible for the performance increase. However, this effect is less clear on CLEVR6.

On CLEVR6, we notice particularly bad metrics for the rotation property. This is not surprising as the rotation parameter is completely useless for two of the three shapes (sphere and cylinder) and redundant for the last one (cube). Because of this bad identifiability and affinity scores thresholding, we can not compute rotation completeness for GENESIS. This does not impact the final metric due to the weighting scheme of our metric. Concerning color channels, we note very different behavior between Multi-dSprites and CLEVR6. We believe that this is due to a particularity of CLEVR6 which

is that the set of color is restricted in the training dataset.

### C.5. Ablation of Algorithm 1

In table 1, we compare the values given by our metric with and without our permutation invariant feature importance algorithm. We observe a significant performance drop for all metrics when the algorithm is ablated from the metric, except for GENESIS. This is consistent with visual inspection of the slot ordering.

## D. Reproducibility

### D.1. Models

**MONet** We train MONet exactly as in (Burgess et al., 2019), except that we set  $\sigma_{fg} = 0.1$  and  $\sigma_{bg} = 0.06$  which was shown to yield better results in (Greff et al., 2019). Besides, we use GECO (Rezende & Viola, 2018) to automatically tune the  $\beta$  parameter during training. The reconstruction constraint was manually set to ensure satisfying visual results (-1.78 for Multi-dSprites, -1.75 for CLEVR6). We found it especially important for the beginning of the training to set a minimum value of 1 for  $\beta$ . Failure to do so resulted in frequent local optima for the representation in which the network was stuck. We used the implementation provided by the authors of (Engelcke et al., 2019). Note that contrary to the latter, we do not include  $\gamma$  in the GECO framework. We use the value of 0.5 given the authors of MONet. The  $\gamma$  parameter controls a mask reconstruction loss, therefore we did not set it to 0 in MONet (R).

**GENESIS** We follow the training process described in (Engelcke et al., 2019) and use the implementation provided by the authors. CLEVR6 is not considered in this paper: we used the same parameters as for Multi-dSprites and changed the reconstruction objective to  $-1.428$ .

**IODINE** We use the parameters described in (Greff et al., 2019). Since the authors did not release their code, we used a third-party implementation.<sup>2</sup> For Multi-dSprites, we had to increase the  $\sigma$  parameter from 0.1 to 0.14 in order to obtain satisfying results with the slight variations in our dataset.

We train all models for 200 epochs. This corresponds to approximately 300 000 updates on Multi-dSprites and 450 000 updates on CLEVR6. Models were trained with one to four V100 GPUs. The training times ranges from a few hours to 1.5 days.

<sup>2</sup>[github.com/zhixuan-lin/IODINE](https://github.com/zhixuan-lin/IODINE)

## D.2. Training datasets

**Multi-dSprites** For training, we use the dataset and pre-processing code from (Engelcke et al., 2019). Note that the datasets contains images composed of 1 to 4 objects, contrary to (Greff et al., 2019) that goes up to 5 objects. This explains the better segmentation values in our setting compared to the latter.

**CLEVR6** We generate the training dataset similarly as in (Greff et al., 2019), with the modification that we add an additional constraint that all objects have to be visible inside the cropped 192x192 image. This modification is important for our metric. It tends to generate slightly denser scenes than in previous work. This might partly explain why we get slightly worse ARI for MONet compared to previous work (0.94 against 0.96). Scenes have at most 6 objects.

## D.3. Evaluation

**Evaluation datasets** The evaluation datasets are sampled in the same way, except that we restrict to images with 4 objects for Multi-dSprites and images with exactly 6 objects for CLEVR6. We sample 10 local groups (see Algorithm 2) for Multi-dSprites and 5 for CLEVR6. Each group has 5000 samples, with a 4000/500/500 split for fitting, validation and evaluation of the factor predictor. In Table 6, we give the list of factors for each individual object in both datasets, with the possible values for each factor.

**Factor prediction** For the temporary predictors in Algorithm 1 (inside the loop), we use a linear model with Ridge regularization. For the final predictor, we use a random forest with 10 trees, and a maximum depth of 15. The is because the random forest obtains better predictions, while the linear model permits faster iterations. The number of iterations of the loop is set to 100 for Multi-dSprites. For computational reasons, we reduced this number to 20 for CLEVR6. This reduction does not harm performance as the vast majority of permutations happen in the first iterations. Most factors are continuous or ordinal: for these, we encode factor prediction as a regression task. The material factor in CLEVR6 has only two classes and we follow the encoding used in sklearn Ridge Classifier. On both datasets, the shape factor has three classes: we generalize the Ridge Classifier encoding and encode the classes as -1, 0 and -1. We match the classes to these values in order to minimize prediction error.

**Metric** In order to filter out noise in the feature importances, we set to 0 to all the relative importance coefficients that are less than 3% of the column maximum in absolute value. In our evaluation of object-level disentanglement, we remove the factors and latent dimensions that are background related. For Multi-dSprites, the background slot is

identified as the one with higher importance in predicting background color. For CLEVR6, there is no background color, but the background is always reconstructed by the first slot in the benchmarked models. The global informativeness metric is an unweighted average over all factors.

Table 3. Ablation of Algorithm 1 for Multi-dSprites. We report mean and std error over three random seeds. All values are in %. 100 is the best possible score and 0 the worst, except for the informativeness metric where 0 is best. All models are trained with variational loss.

MODEL	OBJECT-LEVEL		PROPERTY-LEVEL			
	DIS. (↑)	COMP. (↑)	DIS. (↑)	COMP. (↑)	INF. (↓)	
MONET (ENGELCKE)	52 ± 4	52 ± 4	39 ± 6	60 ± 5	45 ± 3	
MONET (ENGELCKE) (WITHOUT ALG 1)	30 ± 2	30 ± 2	27 ± 4	53 ± 3	51 ± 3	
MONET	75 ± 7	75 ± 7	59 ± 6	<b>74 ± 5</b>	26 ± 6	
MDSPR.	MONET (WITHOUT ALG 1)	40 ± 3	40 ± 4	44 ± 5	65 ± 3	30 ± 6
GENESIS	<b>90 ± 0.8</b>	<b>91 ± 0.6</b>	<b>72 ± 0.5</b>	60 ± 0.4	<b>24 ± 0.4</b>	
GENESIS (WITHOUT ALG 1)	89 ± 0.1	90 ± 0.1	72 ± 0.1	60 ± 0.3	23 ± 0.4	
IODINE	70 ± 9	72 ± 10	37 ± 5	62 ± 4	37 ± 6	
IODINE (WITHOUT ALG 1)	32 ± 2	33 ± 2	21 ± 1	52 ± 1	47 ± 4	

Table 4. Informativeness and Completeness per object property for all models trained with variational loss on Multi-dSprites.

	COMPLETENESS (↑)				INFORMATIVENESS (↓)			
	GENESIS	IODINE	MONET (E)	MONET	GENESIS	IODINE	MONET (E)	MONET
R CHANNEL	91	71	88	94	9	16	5	5
G CHANNEL	90	68	81	89	10	17	6	7
B CHANNEL	90	77	86	96	9	16	4	5
SHAPE	30	49	42	50	26	45	59	34
SCALE	32	49	42	55	38	53	66	41
ORIENTATION	24	48	36	45	31	65	97	62
X	34	59	39	69	36	50	75	36
Y	33	63	39	67	35	48	74	34

Table 5. Informativeness and Completeness per object property for all models trained with variational loss on CLEVR6.

	COMPLETENESS (↑)			INFORMATIVENESS (↓)		
	GENESIS	MONET (E)	MONET	GENESIS	MONET (E)	MONET
R CHANNEL	54	47	47	47	57	61
G CHANNEL	59	50	46	41	58	62
B CHANNEL	61	54	46	38	47	58
SHAPE	27	40	39	64	66	66
MATERIAL	56	56	53	28	39	41
SIZE	49	64	63	24	28	22
ROTATION	NA	36	36	106	107	107
X	27	52	54	38	47	41
Y	31	61	65	30	39	32

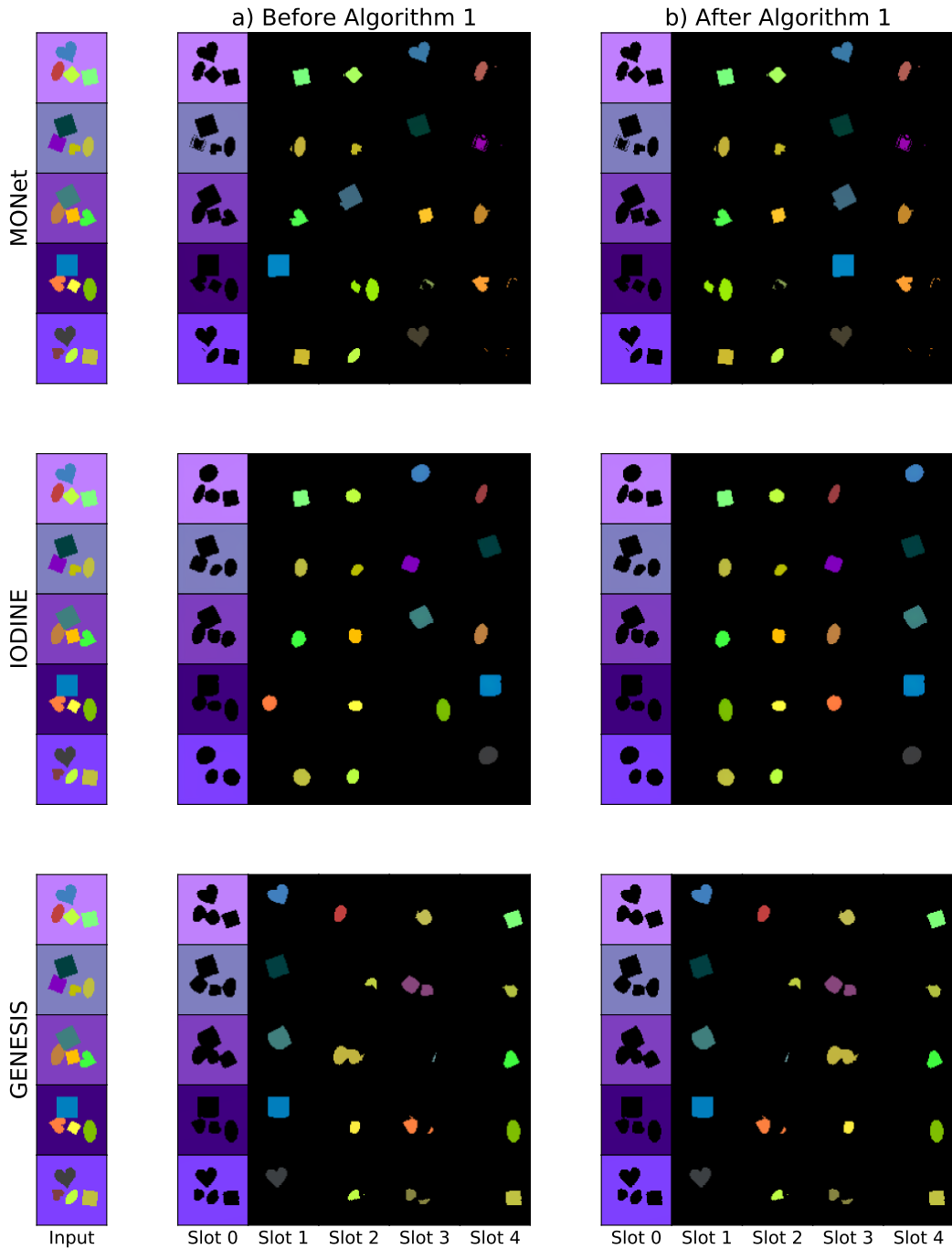


Figure 4. Visualization of the effect of Algorithm 1 on slot ordering for a group of similar inputs.

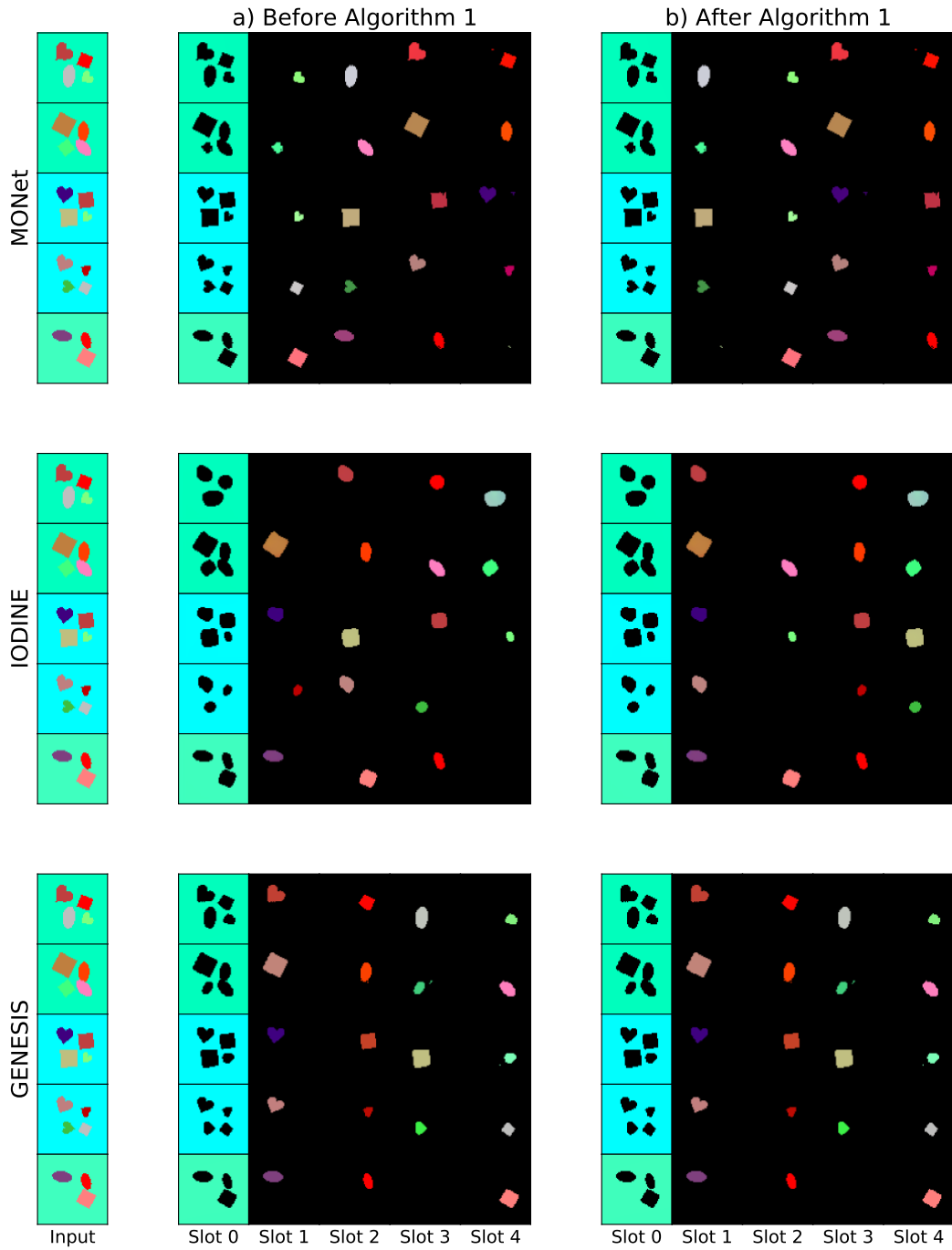


Figure 5. Visualization of the effect of Algorithm 1 on slot ordering for a group of similar inputs.

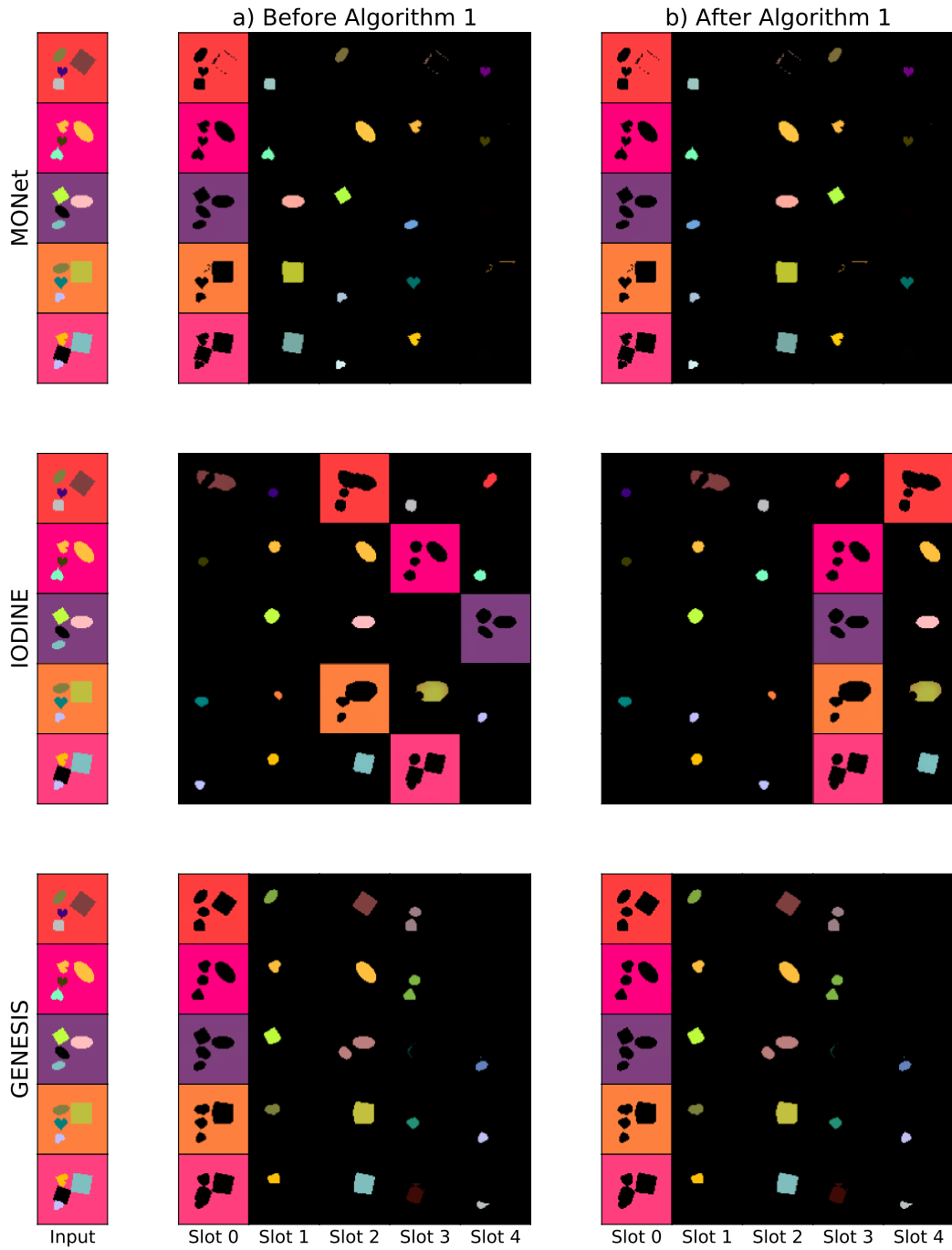


Figure 6. Visualization of the effect of Algorithm 1 on slot ordering for a group of similar inputs.

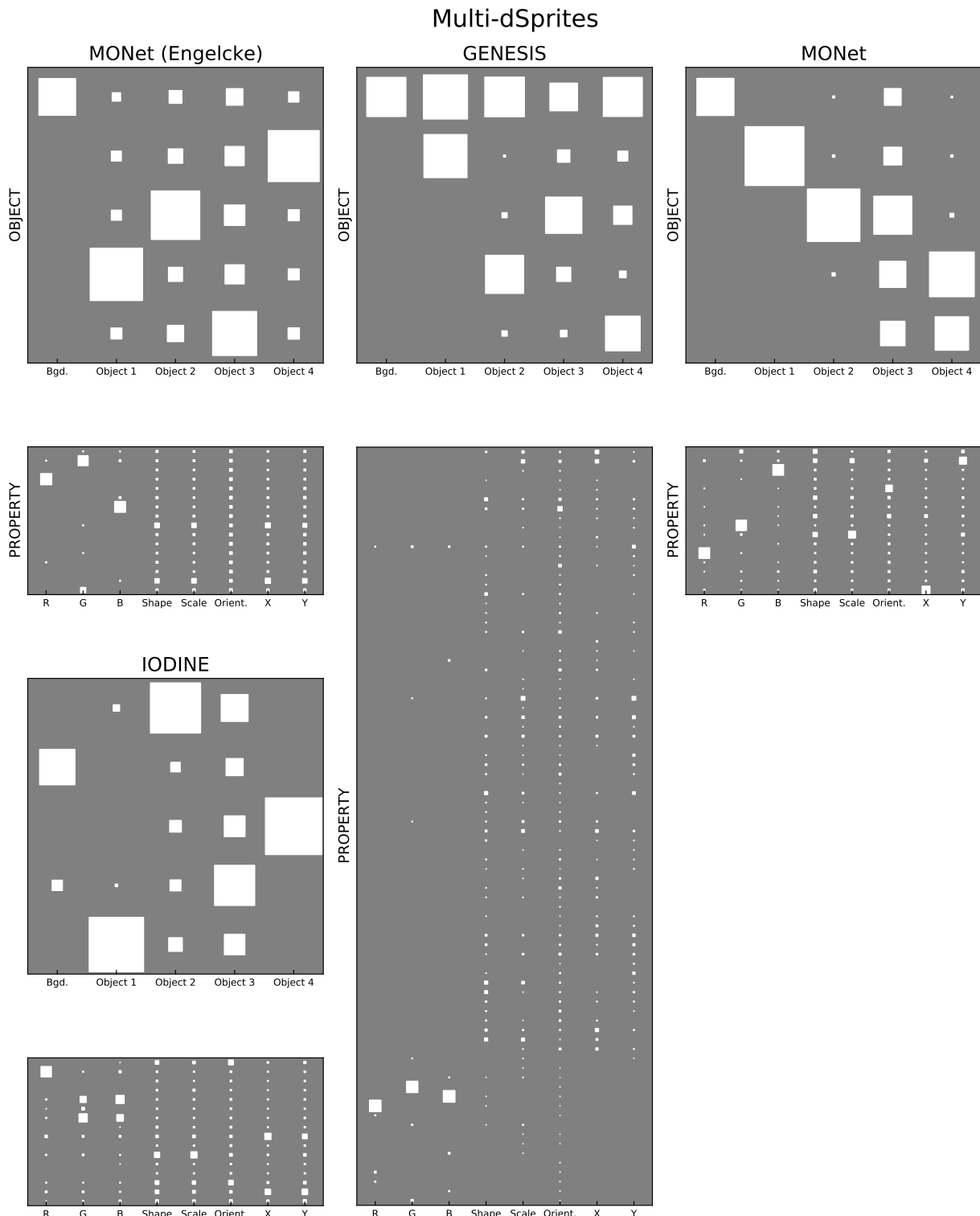


Figure 7. Projections of the affinity matrix at object-level and property-level for all four models trained with variational loss on Multi-dSprites. (Hinton diagram)

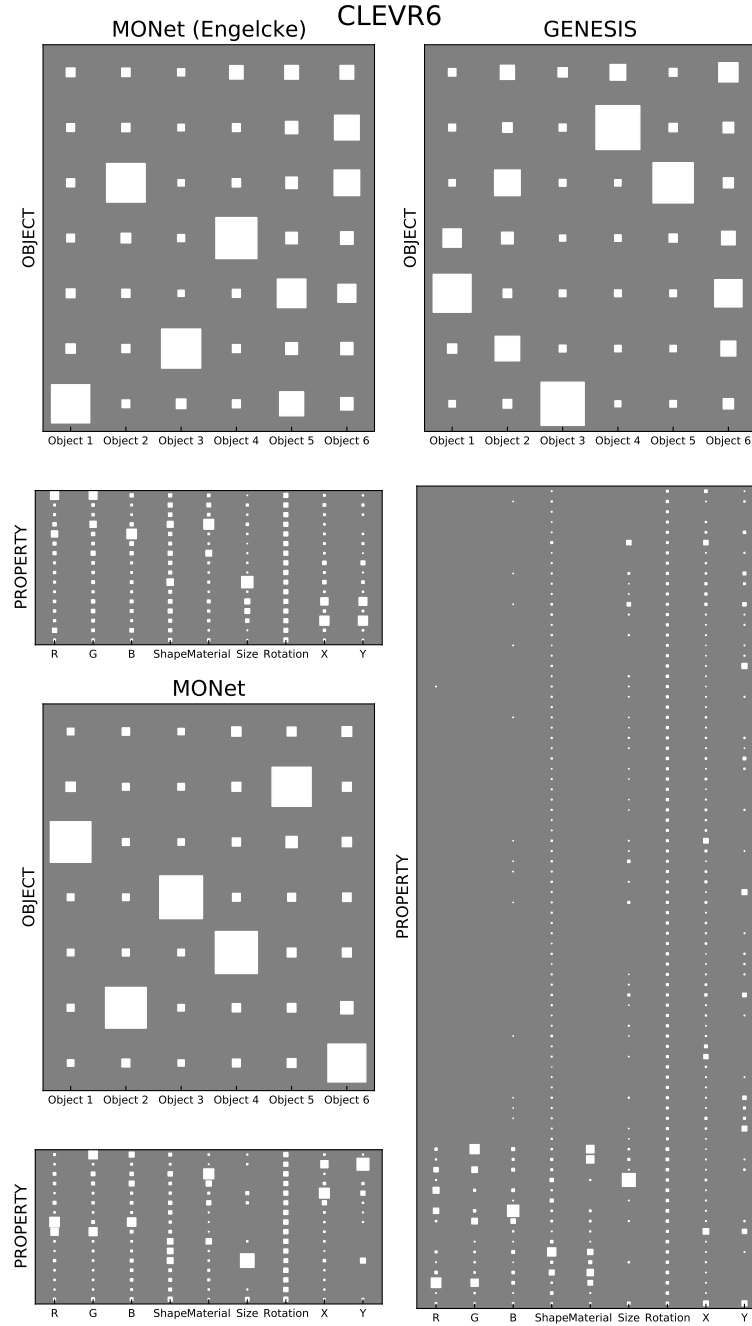


Figure 8. Projections of the affinity matrix at object-level and property-level for all three models trained with variational loss on CLEVR6 (Hinton diagram).

Table 6. Description of the factors of variation for each individual object in both datasets. For each factor, we give the set of possible values, as well as the exact locality constraints used in Algorithm 2.  $x$  denotes the initial value sampled in Algorithm 2. When  $x$  has values in an array, we denote  $i$  the index such that  $x = a[i]$ .

DATASET	OBJECT FACTORS OF VARIATION	TYPE	POSSIBLE VALUES	LOCAL CONSTRAINT (ALG. 2)
MDSPR.	COLOR (R CHANNEL)	INTRINSIC	$[0, 63, 127, 191, 255]$	$[a[i - 1], a[i], a[i + 1]]$
	COLOR (G CHANNEL)	INTRINSIC	$[0, 63, 127, 191, 255]$	$[a[i - 1], a[i], a[i + 1]]$
	COLOR (B CHANNEL)	INTRINSIC	$[0, 63, 127, 191, 255]$	$[a[i - 1], a[i], a[i + 1]]$
	SHAPE	INTRINSIC	{circle, square, heart}	{circle, square, heart}
	SCALE	INTRINSIC	$[0, 1, 2, 3, 4, 5]$	$[a[i - 1], a[i], a[i + 1]]$
	ORIENTATION	EXTRINSIC	$[0, 1, \dots, 30, 39]$	$[a[i - 3], a[i - 2], \dots, a[i + 2], a[i + 3]]$
	X COORD.	EXTRINSIC	$[0, 1, \dots, 30, 31]$	$[a[i - 2], \dots, a[i + 2]]$
CLEVR6	Y COORD.	EXTRINSIC	$[0, 1, \dots, 30, 31]$	$[a[i - 2], \dots, a[i + 2]]$
	COLOR (R CHANNEL)	INTRINSIC	$[0, 0.2, 0.4, 0.6, 0.8, 1]$	$[a[i - 1], a[i], a[i + 1]]$
	COLOR (G CHANNEL)	INTRINSIC	$[0, 0.2, 0.4, 0.6, 0.8, 1]$	$[a[i - 1], a[i], a[i + 1]]$
	COLOR (B CHANNEL)	INTRINSIC	$[0, 0.2, 0.4, 0.6, 0.8, 1]$	$[a[i - 1], a[i], a[i + 1]]$
	SHAPE	INTRINSIC	{cube, sphere, cylinder}	{cube, sphere, cylinder}
	MATERIAL	INTRINSIC	{rubber, metal}	{rubber, metal}
	SIZE	INTRINSIC	$[0.35, 0.7]$	$[0.35, 0.7]$
CLEVR7	ROTATION	EXTRINSIC	$\llbracket 0, 360 \rrbracket$	$\llbracket 0, 360 \rrbracket$
	X COORD.	EXTRINSIC	$\llbracket -3, 3 \rrbracket$	$\llbracket x - 0.7, x + 0.7 \rrbracket \cap \llbracket -3, 3 \rrbracket$
	Y COORD.	EXTRINSIC	$\llbracket -3, 3 \rrbracket$	$\llbracket x - 0.7, x + 0.7 \rrbracket \cap \llbracket -3, 3 \rrbracket$